



## OPEN

# Numerical evaluation of the scale problem on the wind flow of a windbreak

SUBJECT AREAS:

ENVIRONMENTAL  
SCIENCES

GEOMORPHOLOGY

Received  
6 June 2014Accepted  
29 September 2014Published  
14 October 2014Correspondence and  
requests for materials  
should be addressed to  
B.L. (liubenli@lzb.ac.  
cn)Benli Liu<sup>1</sup>, Jianjun Qu<sup>1,2</sup>, Weimin Zhang<sup>1</sup>, Lihai Tan<sup>1</sup> & Yanhong Gao<sup>3</sup>

<sup>1</sup>Dunhuang Gobi Desert Ecological and Engineering Research Station, Key Laboratory of Desert and Desertification, Chinese Academy of Sciences, Lanzhou 730000, China, <sup>2</sup>Gansu Center for Sand Hazard Reduction Engineering and Technology, Lanzhou 730000, China, <sup>3</sup>Key Laboratory for Land Surface Process and Climate Change in Cold and Arid Regions, Chinese Academy of Sciences, Lanzhou 730000, China.

The airflow field around wind fences with different porosities, which are important in determining the efficiency of fences as a windbreak, is typically studied via scaled wind tunnel experiments and numerical simulations. However, the scale problem in wind tunnels or numerical models is rarely researched. In this study, we perform a numerical comparison between a scaled wind-fence experimental model and an actual-sized fence via computational fluid dynamics simulations. The results show that although the general field pattern can be captured in a reduced-scale wind tunnel or numerical model, several flow characteristics near obstacles are not proportional to the size of the model and thus cannot be extrapolated directly. For example, the small vortex behind a low-porosity fence with a scale of 1 : 50 is approximately 4 times larger than that behind a full-scale fence.

A fence is a useful windbreak because of its effect on wind erosion<sup>1–4</sup>, sand movement and deposition<sup>5–7</sup>, microclimate<sup>8,9</sup> and soil conditions<sup>10</sup> (Fig. 1). Many studies have been conducted to study the influence of the shape, height, spacing and porosity of a fence on changes in airflow fields and on the reduction in the leeward wind velocity. Porosity is defined as the ratio of the total pore area to the total fence area. The critical porosity of a fence, below which flow separation and reversal occur, is approximately 0.3 according to previous works<sup>11–13</sup>, whereas its optimal porosity is determined to be approximately 0.3 to 0.4 by most researchers<sup>2,14–16</sup>. Airflow regions behind a low-porosity or solid fence can be identified as: outer flow, overflow, an internal boundary layer, a reverse cell and a small vortex<sup>13</sup>.

Considering the difficulty in capturing the entire flow field around a fence at an actual site, inherent advantages, such as controllability and repeatability, have made wind tunnel experiments one of the most fundamental methods for studying the influence of a fence on airflow and the effect of fence porosity. For detailed investigations, several types of advanced equipment, such as laser Doppler velocimeters, particle tracking velocimeters and particle image velocimeters (PIVs) have been applied by researchers to study the entire airflow field, particularly leeward of fences; such equipment are superior to conventional pitot tube anemometers or hot-wire anemometers<sup>4,5,13,16</sup>. The use of non-intrusive methods is currently limited to wind tunnel experiments because such techniques are inapplicable in the field in terms of releasing fine tracer particles and capturing them at a fixed plane using a charge-coupled device camera.

Key issue in this type of research are determining whether the experiment results are directly applicable to the actual conditions and determining the extent of the result's application based on the following reasons: (1) the fence model in a wind tunnel is typically reduced to the millimetre or centimetre level, (2) the schematic of a porous fence and the materials used are hardly similar to those of an actual windbreak and (3) the roughness heights and inlet wind profiles between a wind tunnel floor and a natural land surface are different. Moreover, the ratio of the measured reference height of inlet wind in a wind tunnel to the height of the model is generally not proportional to that in the field; thus, making it difficult to validate the accuracy of the experiment results under an actual tested wind speed condition. The scale problem has been mentioned by several researchers<sup>17–19</sup>; however, no specific investigation is found in the literature.

An independent method that can conduct a comparison between an experimental model in a wind tunnel and an actual fence, while keeping other boundary conditions similar to their actual conditions, will determine whether the experiment results can be applied to actual situations. Computational fluid dynamics (CFD) simulation provides a possible solution to this issue. CFD has already been proven as a reliable means to study the wind flow field of a windbreak to discuss its protective effect<sup>6,17,20–22</sup> and other complex geometries<sup>23–27</sup>. The literature is also rich with validations of CFD studies on windbreak flow using wind tunnel results<sup>8,28</sup>. However, these previous

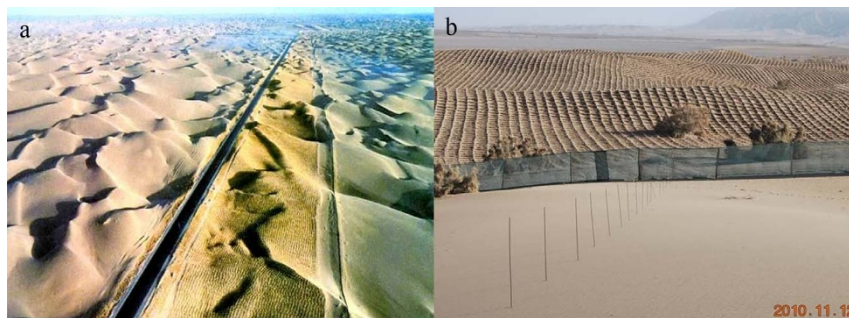


**Figure 1** | Fences in the blowing-sand shelter systems that protect (a) the highway that crosses the Taklimakan Desert (photo taken by Jianjun Qu) and (b) the Dunhuang Mogao Grottoes (photo taken by Weimin Zhang).

works were frequently based on same-scale comparisons. In the present study, we used a CFD simulation method to study the scale effect on mean velocity fields behind fences with different porosities. In particular, we compared the airflow fields of a porous fence model with those of its on-site counterpart.

The wind tunnel experiment performed by Dong et al.<sup>13</sup> was selected as a reference because (1) it presented a high-precision result via PIV and (2) this experiment had a practical application for the fences along the highway of the Taklimakan Desert in China, as shown in Figure 1a. The fence in this wind tunnel experiment has a height of 20 mm ( $H$ ) and a thickness of 1.2 mm; these values represent a 1 m high and 0.06 m thick reed-bunch fence with a geometric scale of 1 : 50. A numerical fence model with the same size in the same wind tunnel experiment was developed 14  $H$  after the inlet and 26  $H$  before the outlet. The height of the simulation domain was set to 12  $H$ , which was sufficient for the complete development of the airflow. To understand how the airflow characteristics around the fence change with different scales, the model was magnified 50 times to represent the actual scenario.

An inlet wind profile was provided by the following logarithmic law:

$$u(z) = u^* / \ln(z/z_0), \quad (1)$$

where  $u(z)$  is the wind speed value at a  $z$ (m) height,  $k = 0.41$  is the von Karman coefficient,  $u^*$  is the friction velocity and  $z_0$  is the surface roughness. Four wind speed conditions, i.e., 8 m/s, 10 m/s, 12 m/s, and 14 m/s, were considered at a 30 cm height in the wind tunnel scenario and a 2 m height in the actual scenario. A value of  $z_0 = 0.004$  mm was used in the wind tunnel simulation based on the measured wind profiles in the wind tunnel, whereas  $z_0 = 0.001$  cm, which is a typical value over a blown sand surface, was used in the actual scenario.

We developed nine porosity scenarios ( $\eta = 0, 0.05, 0.1, 0.15, 0.2, 0.3, 0.4, 0.5$  and  $0.6$ ). Conditions in which the porosity exceeds 0.6 were not considered because previous works show that the porosity effect is weak above these values. A total of 72 simulation cases are required for the four wind speed conditions and the two scale levels for each fence. The fence can be regarded as a thin porous boundary that acts as a momentum sink and causes a pressure drop  $\Delta P$  in the flow passing through it:

$$\Delta P = 0.5k_r \rho v^2, \quad (2)$$

where  $v$  is the normal velocity toward the fence,  $k_r$  is the pressure loss coefficient related to the porosity of the fence and  $\rho$  is the air density.

The porosity values were defined by changing the  $k_r$  of the fence instead of the solid model itself. To estimate the pressure loss coefficient at various fence porosity conditions, two common empirical relationships are available. One of these relationships was from Reynolds<sup>29</sup>, i.e.,

$$k_r = 0.52(1 - \eta^2) / \eta^2, \quad (3)$$

whereas the other relationship was from Hoerner<sup>30</sup>, i.e.,

$$k_r = 0.5(3/2\eta - 1)^2. \quad (4)$$

The estimation results from the two relationships have the same change patterns given that the  $k_r$  values of both are related to  $1/\eta^2$ . The results from the Reynolds equation are smaller when  $\eta < 0.06$ , and vice versa, with limited absolute differences. However, the relative differences are significant at large porosity conditions, reaching approximately 40% when  $\eta = 0.6$ . To reduce errors from the estimation, the average results from the two equations were adopted in our simulations. Moreover, the permeability of the fences was set to a high value of  $10^{10}$  m<sup>2</sup> to cancel out viscous effects.

The current study may be the first to simulate flow around porous wind fences at different scale scenarios to test the scale problem. As a standard procedure to validate the numerical method and the applicability of the turbulence model, the results of the current study were first compared with the PIV-measured wind tunnel results. If the simulation results were directly comparable with those of the wind tunnel study, then the scale problem of a reduced numerical or wind tunnel model can be discussed. The scale effect was evaluated by comparing wind speed contours and wind profiles at 13 locations ( $-2, -1, -0.5, 0.5, 1, 2, 4, 6, 9, 12, 16, 20,$  and  $25 H$ ) in the wind tunnel-sized simulations with those from the actual-sized simulations.

## Results

**Comparison with the previous wind tunnel experiment.** The flow field behind a porous fence can be characterised by the shape and size of the reverse cell, the location of the flow separation zone and the flow speed at several specific locations. The flow convergence distance on the leeward side of the fence, which is where the forward flow and reversed backward flow meet to form a zero-speed contour, was sensitive to changes in the fence porosity. The comparison between the flow convergence length from the wind tunnel and the CFD simulation at the two fence scales is shown in Fig. 2. The experiment results are consistent with those of the scaled simulation. A general trend in which the convergence length increased with the wind porosity was observed for all wind speed conditions, except for the wind tunnel result with a wind speed of 8 m/s and  $\eta = 0.2$ . This abnormal value may have resulted from an experimental error.

Similar to many previous studies, the CFD-simulated flow field characteristics, including streamline patterns, velocity profiles and flow regions, are consistent with the results of the wind tunnel experiments; thus, the applicability of the numerical method is proven. In addition, Dong et al.<sup>13</sup> noted that the convergence length does not increase when the porosity is lower than 0.05. The simulation at the wind tunnel model scale exhibited the same features at all wind speed conditions, further proving that the CFD method could represent the flow field with high precision and reliability. However, the simulation with an actual-sized model resulted in an obviously low relative length when the porosity was less than 0.1 and a high value when

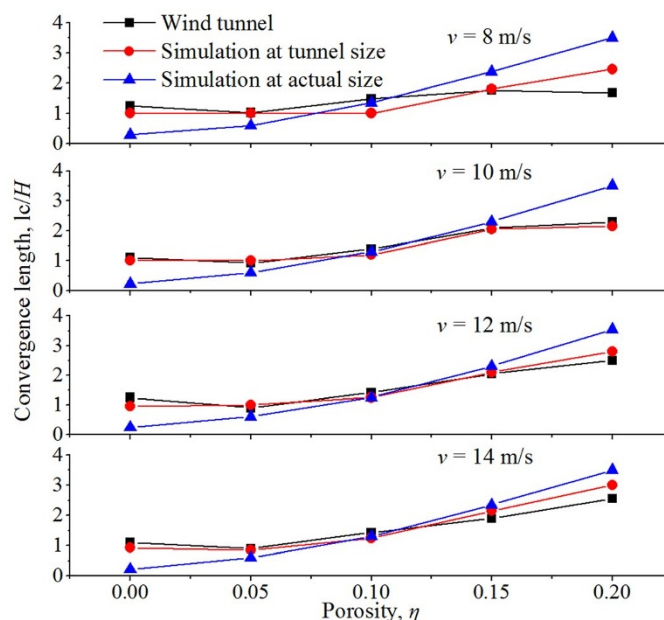


**Figure 2** | Comparison between the flow convergence length from the wind tunnel experiment and the CFD simulation at the two scales.

the porosity was larger than 0.15. This finding was affected by the different relative intensities of a small vortex that occurred immediately behind the fence at low porosity conditions.

A small vortex behind a solid or low-porosity fence was observed in the wind tunnel<sup>13</sup> and in both numerical simulations in the present study. A direct comparison of the vortex in the two scale simulations reveals the difference caused by the scale effect (Fig. 3). Under a 10 m/s wind condition, the vortex behind the solid wind tunnel model fence was well developed to approximately a  $0.6 H$  height and  $1 H$  distance, whereas the vortex behind the actual size solid fence had a height and distance of only approximately  $0.15 H$  and  $0.25 H$ , respectively; the relatively small vortex in the latter led to the short convergence length of the actual-sized simulation in Fig. 2. If the measured wind tunnel and CFD-simulated data were extrapolated 50 times to their actual size, then the height and length of the vortex would be 4 times larger than those of the vortex in the actual-sized model. This scale-affected difference indicates that although the general flow characteristics can be captured using scale models in a wind tunnel or same-scale CFD simulations, as tested by many previous works, the results of these methods will not be proportional to the model size and can be deformed if applied directly to a unique area, particularly near obstacles.

**Comparison of flow fields at two scaled fences.** In the current study, we focused on changes in flow velocity that were caused by different model scales. First, the result shows that the wind speed had a limited effect on the flow pattern, as proven by many previous studies. For each scale and porosity scenario at 13 locations, the wind profiles under four referential wind speeds were proportional and highly correlated with one another ( $r = 1$ ). The percentage differences in the wind velocity of the two scale simulations were calculated by averaging the difference at each measured location under the four wind speed conditions. The average percentage difference at each porosity scenario was then determined by obtaining the average of the differences at all the measured locations.

A direct comparison between the flow fields behind the two scaled fences revised several general similarities and differences caused by the scale effect. The lift streamline that approached the fence, the flow compression above the fence, the bleed flow immediately after the fence, the high-velocity region above the fence, the flow reattachment distance and the shape of the separation cell for the two scale simulations are consistent, as shown in Fig. 4 for a porosity of 0.3 and an inlet wind speed of 10 m/s.

However, a significant difference was observed, i.e., the overall wind speed in the actual-sized simulation was apparently higher than

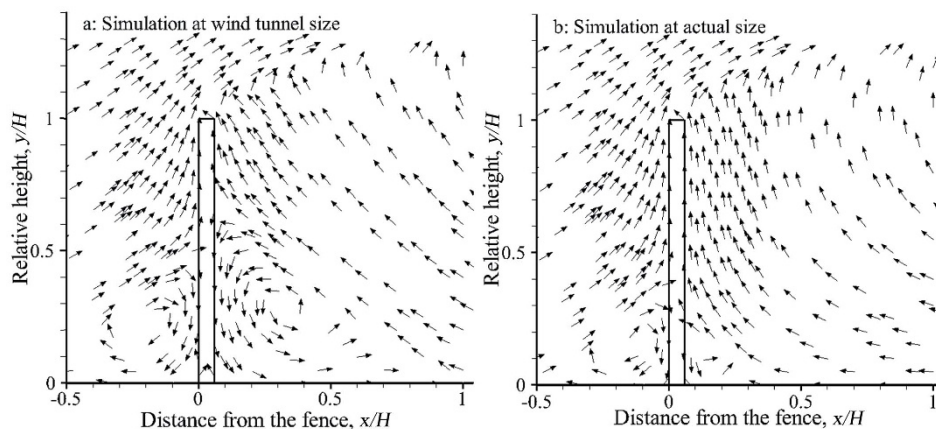


**Figure 3** | Comparison of the small vortex behind a solid fence at the two scales; wind speed = 10 m/s and  $\eta = 0$ .

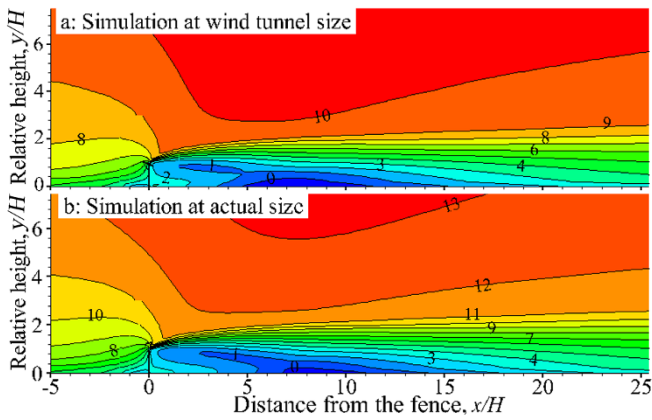


**Figure 4** | Comparison between the flow contours behind a fence at two scales, where  $\eta = 0.3$  and  $v = 10$  m/s.

that in the wind tunnel-sized simulation (Fig. 4). This finding is attributed to the referential wind speed in the wind tunnel that was monitored as 0.3 m (15  $H$ ) above the surface, whereas in the actual-sized simulation, the speed was 2 m high, which corresponds to 2  $H$  as the typical field condition. Another difference was observed in the varying relative strengths of the bleed flow behind the porous fence. In the actual-sized simulation, the space for the bleed flow development was larger, and lead to a longer convergence length and a more intensive leeward deformation of the separation cell. In contrast, the space behind the 20 mm-high wind tunnel fence was limited; thus, the intensity of the bleed flow was smaller behind the fence.

A quantitative comparison of the wind profiles at various locations emphasised that the difference in the outer-flow and overflow zones was caused by the varying ratios of the referential wind speed height to the fence models and by the displacement of small vortices or reverse cells leeward (Fig. 5). At the 13 compared locations, the difference in the total wind speed of the 9 porous conditions was 21.1%, which was close to the average wind speed difference of 22.9% from the inlet boundaries. The data are stable at the outer-flow and overflow regions, as well as behind the separation cells. However, the

data fluctuate, with large standard deviations, behind the fence that was affected by high-intensity turbulence, particularly near or within a small vortex and before the separation cell of low porosity fences because the absolute wind speed is low and the two flow patterns differ in these areas; thus, a small difference in values can result in a highly variable ratio. These differences indicate that the results from the wind tunnel simulation at a certain referential wind speed or for particular characteristics in a scale model are not directly applicable to the actual condition, even when the same inlet wind speed is assumed. The results also reiterate that the porous effect ceases when  $\eta$  is larger than 0.5.

## Discussion

This study presents the first numerical analysis of the scale problem of a windbreak in wind tunnel experiments and reduced-scale simulations. The flow field difference that was influenced by the scale effect between the two fence models was numerically measured. The result of the comparison between the wind tunnel experiment and the CFD simulation with an equal size is encouraging, and emphasizes the reliability of the CFD method. However, two major differences between the flow fields of the scale model and the actual-sized fence were determined.

In the outer-flow and overflow regions where the fence had limited influence, the difference was mainly caused by the varying ratios of the referential wind speed heights in the model and of the actual-sized fences. This problem is common because a wind tunnel model is typically scaled down tens or several hundred times from the actual size, which can be generally solved by considering referential wind speed height and model size, for example, by multiplying by approximately 122% in the current study.

Moreover, the small vortex and the separation cell behind a low-porosity fence are not proportional to the size of the model; thus, a significant discrepancy occurs between the wind tunnel and the actual-sized simulations immediately behind the fence and within the separation cell. For example, the small vortex behind a low-porosity fence is relatively four times larger in the 1 : 50 scale model. This problem can only be addressed by comparing two numerical models at the required scales and then extrapolating the results of a wind tunnel experiment to the actual condition.

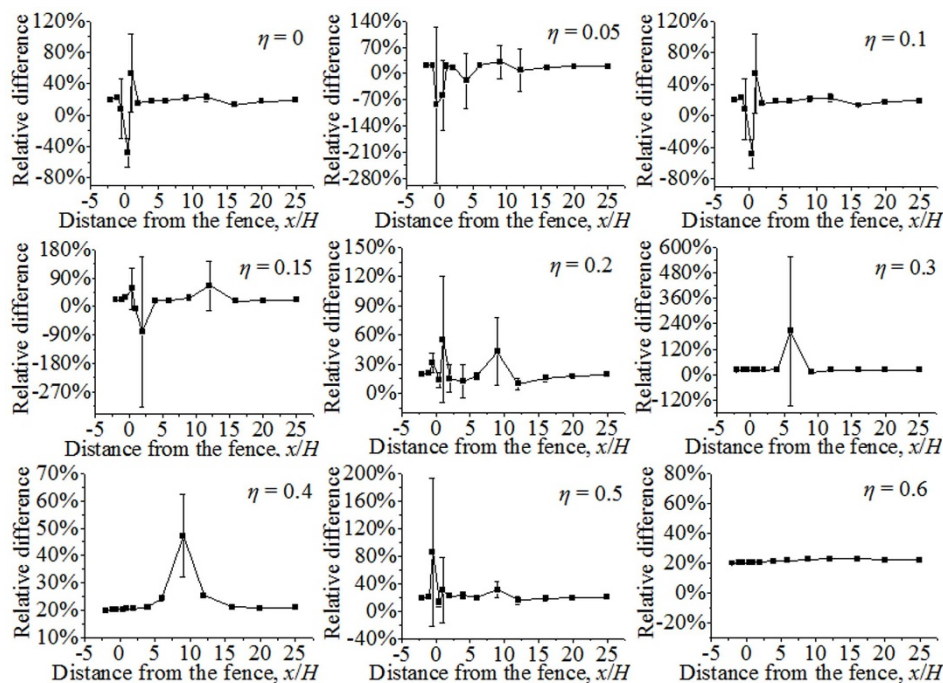


**Figure 5** | Average wind speed differences at the 13 compared locations of the two scale simulations under 9 porosity conditions.



## Methods

ANSYS Fluent code (version 12.0), which was frequently used in previous studies, was also used in our simulations. Fluid (air) is considered incompressible and Newtonian. The shear stress transport (SST)  $k-\omega$  turbulence model was used to provide closure. The SST model automatically changes from the standard turbulence/frequency-based  $k-\omega$  model in the inner region of the boundary to a higher Reynolds number  $k-\epsilon$  model in the bulk flow. The accuracy and reliability of this model can be increased for a broader class of flows than the standard  $k-\epsilon$  and  $k-\omega$  models<sup>31</sup>.

**Boundary conditions.** The wind profile given in equation (1) was imposed as the inlet boundary condition with a changing  $u^*$  to alter the referential wind speed, whereas for the top boundary the inlet velocity at its height was assigned. The non-slip boundary condition was applied to the floor with  $z_0$ , as described previously. The zero-pressure boundary condition was adopted for the outlet boundary. The porous condition of the fence was applied according to the  $k_f$ , calculated from equations (3) and (4) and the width of the fence. The solid fence with a porosity of 0 was modelled as a wall.

**Discretisation scheme and specifications of the turbulence model.** The fully developed turbulent wind flow over the fence was solved by the Reynolds-averaged Navier-Stokes equations that use the finite volume method. The default “standard wall function” applied the wall boundary condition to all variables of the  $k-\omega$  model that were consistent with the logarithmic wind profile in equation (1). The SIMPLEC algorithm was used to solve pressure-velocity coupling. The pressure interpolation scheme was PREssure STaggering Option (PRESTO!). Second-order discretisation schemes were used for the convection and viscous terms of the governing equations. The least-squares cell-based gradient reconstruction scheme was used because of its accuracy and speed. A structured quadrilateral grid method was used in the upstream and downstream regions, whereas an unstructured triangular grid was built near the fence model to bridge fine cells at the bottom of the domain and coarse cells at the top. The grid resolution was determined via grid-sensitivity analyses; thus, the results were independent of the grid size. The total number of cells was 5,100.

The initial conditions for pressure and velocity were set to zero for the entire domain, except at the left inlet boundary wherein the logarithmic wind profile was imposed. The transport equations for the SST  $k-\omega$  model were then solved iteratively until the convergence criteria were satisfied. The convergence criteria were defined in terms of residuals, i.e., the degree to which the conservation equations were satisfied throughout the flow field. We assumed that convergence was achieved when all normalised residuals for the velocity components  $k$  and  $\omega$  fall below  $10^{-5}$ . The execution time of each run was approximately 15 minutes on a 3.40 GHz Intel i7-4770 processor with 8 GB of RAM.

- Borges, A. R. & Viegas, D. X. Shelter effect on a row of coal piles to prevent wind erosion. *J. Wind Eng. Ind. Aerodyn.* **29**, 145–154 (1988).
- Lee, S.-J. & Lim, H.-C. A numerical study on flow around a triangular prism located behind a porous fence. *Fluid Dyn. Res.* **28**, 209–221 (2001).
- Guo, L. & Maghirang, R. G. Numerical simulation of Airflow and Partical collection by vegetative barriers. *Eng. Appl. Comput. Fluid Mech.* **6**, 110–122 (2012).
- Zhang, N., Kang, J.-H. & Lee, S.-J. Wind tunnel observation on the effect of a porous wind fence on shelter of saltating sand particles. *Geomorphol.* **120**, 224–232 (2010).
- Tsukahara, T., Sakamoto, Y., Aoshima, D., Yamamoto, M. & Kawaguchi, Y. Visualization and laser measurements on the flow field and sand movement on sand dunes with porous fences. *Exp. Fluid.* **52**, 877–890 (2011).
- Chen, G., Wang, W., Sun, C. & Li, J. 3D numerical simulation of wind flow behind a new porous fence. *Powder Technol.* **230**, 118–126 (2012).
- Alhajraf, S. Computational fluid dynamic modeling of drifting particles at porous fences. *Environ. Model. Software* **19**, 163–170 (2004).
- Li, W., Wang, F. & Bell, S. Simulating the sheltering effects of windbreaks in urban outdoor open space. *J. Wind Eng. Ind. Aerodyn.* **95**, 533–549 (2007).
- Guan, D., Zhang, Y. & Zhu, T. A wind-tunnel study of windbreak drag. *Agric. For. Meteorol.* **118**, 75–84 (2003).
- Vigiak, O., Sterk, G., Warren, A. & Hagen, L. J. Spatial modeling of wind speed around windbreaks. *CATENA* **52**, 273–288 (2003).
- Perera, M. D. A. E. S. Shelter behind two-dimensional solid and porous fences. *J. Wind Eng. Ind. Aerodyn.* **8**, 93–104 (1981).
- Castro, I. P. Wake characteristics of two-dimensional perforated plates normal to an air-stream. *J. Fluid Mech.* **46**, 599–609 (1971).
- Dong, Z., Luo, W., Qian, G. & Wang, H. A wind tunnel simulation of the mean velocity fields behind upright porous fences. *Agric. For. Meteorol.* **146**, 82–93 (2007).
- Santiago, J. L., Martín, F., Cuerva, A., Bezdeneznykh, N. & Sanz-Andrés, A. Experimental and numerical study of wind flow behind windbreaks. *Atmos. Environ.* **41**, 6406–6420 (2007).

- Park, C.-W. & Lee, S.-J. Verification of the shelter effect of a windbreak on coal piles in the POSCO open storage yards at the Kwang-Yang works. *Atmos. Environ.* **36**, 2171–2185 (2002).
- Lee, S.-J. & Kim, H.-B. Laboratory measurements of velocity and turbulence field behind porous fences. *J. Wind Eng. Ind. Aerodyn.* **80**, 311–326 (1999).
- Yeh, C.-P., Tsai, C.-H. & Yang, R.-J. An investigation into the sheltering performance of porous windbreaks under various wind directions. *J. Wind Eng. Ind. Aerodyn.* **98**, 520–532 (2010).
- Meroney, R. N. CFD prediction of cooling tower drift. *J. Wind Eng. Ind. Aerodyn.* **94**, 463–490 (2006).
- Richardson, G. M. & Richards, P. J. Full-scale measurements of the effect of a porous windbreak on wind spectra. *J. Wind Eng. Ind. Aerodyn.* **54/55**, 611–619 (1995).
- Cong, X. C., Cao, S. Q., Chen, Z. L., Peng, S. T. & Yang, S. L. Impact of the installation scenario of porous fences on wind-blown particle emission in open coal yards. *Atmos. Environ.* **45**, 5247–5253 (2011).
- Fang, F.-M. & Wang, D. Y. On the flow around a vertical porous fence. *J. Wind Eng. Ind. Aerodyn.* **67**, 415–424 (1997).
- Bourdin, P. & Wilson, J. D. Windbreak Aerodynamics: Is Computational Fluid Dynamics Reliable? *Bound. Meteorol.* **126**, 181–208 (2007).
- Mendoza, M., Succi, S. & Herrmann, H. J. Flow Through Randomly Curved Manifolds. *Sci. Rep.* **3**, doi:10.1038/srep03106 (2013).
- Liu, B., Qu, J., Zhang, W. & Qian, G. Numerical simulation of wind flow over transverse and pyramid dunes. *J. Wind Eng. Ind. Aerodyn.* **99**, 879–888 (2011).
- Araujo, A. D., Parteli, E. J. R., Poschel, T., Andrade, J. S. & Herrmann, H. J. Numerical modeling of the wind flow over a transverse dune. *Sci. Rep.* **3**, doi:10.1038/srep02858 (2013).
- Liu, B., Qu, J., Niu, Q., Wang, J. & Zhang, K. Computational fluid dynamics evaluation of the effect of different city designs on the wind environment of a downwind natural heritage site. *J. Arid Land* **6**, 69–79 (2014).
- Stovern, M. *et al.* Simulation of windblown dust transport from a mine tailings impoundment using a computational fluid dynamics model. *Aeolian Res.* doi:http://dx.doi.org/10.1016/j.aeolia.2014.02.008.
- Bitog, J. P. *et al.* Numerical simulation of an array of fences in Saemangeum reclaimed land. *Atmos. Environ.* **43**, 4612–4621 (2009).
- Reynolds, A. J. Flow Deflection by Gauze Screens. *J. Mech. Eng. Sci.* **11**, 290–294 (1969).
- Hoerner, S. F. *Fluid-dynamic drag: practical information on aerodynamic drag and hydrodynamic resistance*, (Brick Town, N. J., 1965).
- Bai, L., Spence, R. R. & Dudziak, G. Investigation of the influence of array arrangement and spacing on tidal energy converter (TEC) performance using a 3-dimensional CFD model. In *Proceedings of the 8th European Wave and Tidal Energy Conference*, Uppsala, Sweden. 654–660 (2009).

## Acknowledgments

We thank Dr. Tianli Bo for the informative discussions on wind profile inhomogeneity in a wind tunnel. This work was supported by the nonprofit industry special research funds from the Chinese Ministry of Water Resources (201201047, 201201048), China Postdoctoral Science Foundation (2014M550518), the Opening Fund of the Key Laboratory of Land Surface Process and Climate Change in Cold and Arid Regions (LPCC201301) and the West Light program for Talent Cultivation of Chinese Academy of Sciences.

## Author Contributions

B.L. and J.Q. designed the study and wrote the manuscript. W.Z. and L.T. participated in the numerical simulations. Y.G. analysed the data and reviewed the manuscript.

## Additional information

**Competing financial interests:** The authors declare no competing financial interests.

**How to cite this article:** Liu, B., Qu, J., Zhang, W., Tan, L. & Gao, Y. Numerical evaluation of the scale problem on the wind flow of a windbreak. *Sci. Rep.* **4**, 6619; DOI:10.1038/srep06619 (2014).



This work is licensed under a Creative Commons Attribution-NonCommercial-ShareAlike 4.0 International License. The images or other third party material in this article are included in the article's Creative Commons license, unless indicated otherwise in the credit line; if the material is not included under the Creative Commons license, users will need to obtain permission from the license holder in order to reproduce the material. To view a copy of this license, visit <http://creativecommons.org/licenses/by-nc-sa/4.0/>